PROCEEDINGS of the
23rd International Congress on Acoustics
9 to 13 September 2019 in Aachen, Germany

Beyond phase grating diffusers using locally-resonant metamaterials

Noé Jiménez[(1)], Trevor J. Cox[(2)], Jean-Philippe Groby[(3)], Vicente Romero-García[(3)]

[(1)]Instituto de Instrumentación para Imagen Molecular, CSIC-UPV, Valéncia, Spain, nojigon@upv.es
[(2)]Acoustics Research Centre, University of Salford, Salford, UK
[(3)]Laboratoire d'Acoustique de l'Université du Maine - CNRS UMR 6613, Le Mans, France

Abstract

We present sound diffusers based on locally resonant metamaterials that are one order magnitude thinner than the classical designs based on phase gratings. Using a set of waveguides loaded by an array of optimized Helmholtz resonators, we induce strong dispersive propagation inside the material. Doing this, waves in the low-frequency regime are dramatically slowed down and, because of this, a deep-subwavelength resonance is produced. In addition, this design allows an accurate tuning of the thermoviscous loses. In this way, the reflection coefficient can be spatially tuned in both phase and magnitude, and we are able to mimic the classical QRD, PRD or Binary/Ternary sound diffusers. Beyond these designs, we also propose an optimized panel showing efficient and broadband sound diffusion ranging from 250 Hz to 2 kHz using only 3 cm thickness, i.e., 46 times thinner than the wavelength at the lowest working frequency.

Keywords: Sound diffusers, Metamaterials, Metasurfaces, Metadiffusers.

1 INTRODUCTION

Sound diffusers are often locally-reacting reflecting surfaces with spatially dependent reflection coefficient usually designed to produce a uniform scattering pattern, i.e., the reflected waves by these surfaces are dispersed in a broad range of directions [1]. To produce such a uniform far field scattering distribution, the spatially dependent reflection coefficient of the panel should present a Fourier transform of uniform magnitude. This was traditionally achieved by using phase grating diffusers, also known as Schröeder's diffusers [2]. These surfaces are rigid-backed slotted panels where each slit acts as a quarter wavelength resonator. However, this approach results in very thick and heavy panels, limiting the use of phase grating diffusers at low-frequencies where the wavelength of sound in air is of the order of several meters [1].

To overcome this limitation, we present *metadiffusers*, sound diffusers based on metamaterials [3]. These structures are composed by optimized air cavities producing slow-sound conditions when waves propagate around their resonances. Metamaterials based on slow sound condition have been widely used to design acoustic absorbers [4, 5, 3, 6]. Using slow sound results in a decrease of the cavity resonance frequency and, hence, the structure thickness can be drastically reduced to the deep-subwavelength regime [5]. Therefore, the thickness of the panel can be reduced to the deep subwavelength regime.

Here, we present deep-subwavelength thickness diffusers based on acoustic metamaterials to reduce the thickness of Schröeder diffusers. The system works as follows: first, we consider a rigid panel of finite length with a set of N slits. Second, we modify the dispersion relations inside each slit by loading one of their walls with a set of Helmholtz resonators, as shown in Fig. 1 (b). The sound propagation becomes strongly dispersive in each slit and the resulting sound speed, c_p, is drastically reduced. Therefore, each slit behaves as a deep-subwavelength resonator. As a consequence, the effective depth of the slits can be strongly reduced as $L = c_p/4f$ holds. By tuning the geometry of the Helmholtz resonators and the thickness of the slits, the dispersion relations inside each slit can be modified. As a result, the phase of the reflection coefficients can be tailored to those of an Schröeder phase grating diffuser, or can be optimized to obtain broadband sound diffusers.

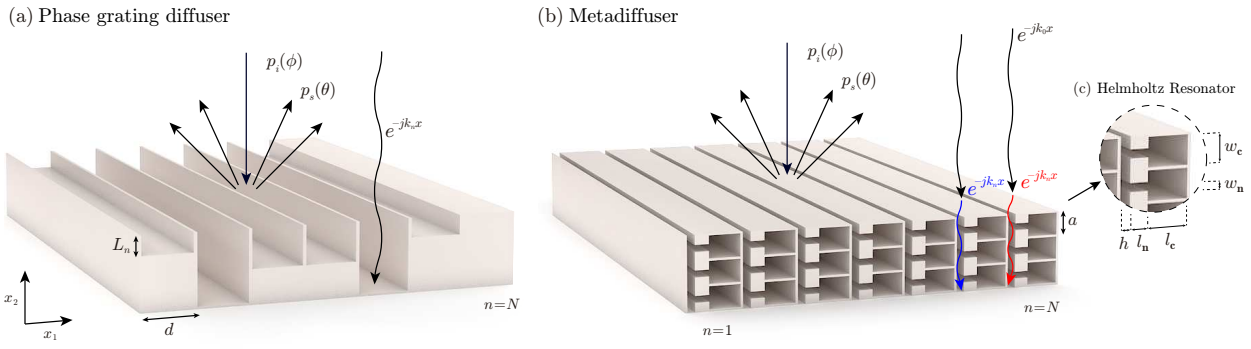


Figure 1. (a) Scheme of a QRD Schröeder diffuser composed by $N = 7$ slits or quarter wavelength resonators. (b) Metadiffuser composed of $N = 7$ sub-wavelength slits, each of them loaded by $M = 3$ Helmholtz resonators, with slightly different geometry.

2 METHODS

2.1 Transfer matrix method

The system described before has been theoretically modelled by using the transfer matrix method. Under the assumption of plane waves travelling inside the metamaterial, either the transfer matrix or the scattering matrix can be obtained, providing directly the reflection of the metamaterial, as well as its effective parameters.

The transfer matrix is used to relate the sound pressures (P) and normal acoustic particle velocities (V) at the beginning and at the end of each slit. The transfer matrix of the n-th slit, $\mathbf{T}^n$, of length L, extending from $y = 0$ to $y = L$ is written as

$$\begin{bmatrix} P^n \\ V^n \end{bmatrix}_{y=0} = \mathbf{T}^n \begin{bmatrix} P^n \\ V^n \end{bmatrix}_{y=L} = \begin{bmatrix} T_{11}^n & T_{12}^n \\ T_{21}^n & T_{22}^n \end{bmatrix} \begin{bmatrix} P^n \\ V^n \end{bmatrix}_{y=L}. \tag{1}$$

For an identical set of M resonators, the transmission matrix $\mathbf{T}^n$ is written as

$$\mathbf{T}^n = \begin{bmatrix} T_{11}^n & T_{12}^n \\ T_{21}^n & T_{22}^n \end{bmatrix} = \mathbf{M}_{\Delta l_{\text{slit}}}^n \left(\mathbf{M}_{\mathbf{s}}^n \mathbf{M}_{\text{HR}}^n \mathbf{M}_{\mathbf{s}}^n\right)^M .$$

Here, the transmission matrix for each lattice step in the n-th slit, $\mathbf{M}_{\mathbf{s}}^n$, is written as

$$\mathbf{M}_{\mathbf{s}}^n = \begin{bmatrix} \cos\left(k_{\mathbf{s}}^n \frac{a}{2}\right) & iZ_{\mathbf{s}}^n \sin\left(k_{\mathbf{s}}^n \frac{a}{2}\right) \\ \frac{i}{Z_{\mathbf{s}}^n} \sin\left(k_s^n \frac{a}{2}\right) & \cos\left(k_{\mathbf{s}}^n \frac{a}{2}\right) \end{bmatrix}, \tag{2}$$

where the slit characteristic impedance is written as $Z_{\mathbf{s}}^n = \sqrt{\kappa_{\mathbf{s}}^n \rho_{\mathbf{s}}^n}/S_{\mathbf{s}}^n$ and $S_{\mathbf{s}}^n = h^n a$, the complex wavenumber is $k_s^n = \omega\sqrt{\rho_{\mathbf{s}}^n/\kappa_{\mathbf{s}}^n}$ and $\kappa_{\mathbf{s}}^n$ and $\rho_{\mathbf{s}}^n$ are the complex and frequency dependent bulk modulus and density in each slit, i.e., the effective acosutic parameters. The resonators are introduced as punctual scatters by a transmission matrix $\mathbf{M}_{\text{HR}}^n$ as

$$\mathbf{M}_{\text{HR}}^n = \begin{bmatrix} 1 & 0 \\ 1/Z_{\text{HR}}^n & 1 \end{bmatrix}, \tag{3}$$

and the radiation correction of the n-th slit to the free space as

$$\mathbf{M}_{\Delta l_{\text{slit}}}^n = \begin{bmatrix} 1 & Z_{\Delta l_{\text{slit}}}^n \\ 0 & 1 \end{bmatrix}, \tag{4}$$

with the characteristic radiation impedance of the n-th slit $Z^n_{\Delta l_{\text{slit}}} = -i\omega\Delta l^n_{\text{slit}}\rho_0/\phi_t^n S_0$, where $S_0 = d\,a$, ρ_0 the air density and Δl^n_{slit} the proper end correction that will be described later.

Finally, the reflection coefficient of the rigidly backed slit can be directly calculated from the elements of the matrix $\mathbf{T}^n$ as

$$R^n = \frac{T^n_{11} - Z_0 T^n_{21}}{T^n_{11} + Z_0 T^n_{21}}. \tag{5}$$

with $Z_0 = \rho_0 c_0/S_0$, and finally the absorption as $\alpha^n = 1 - |R^n|^2$. The effective parameters of each slit can be obtained from the transfer matrix elements as follows

$$k^n_{\text{eff}} = \frac{1}{L}\cos^{-1}\left(\frac{T^n_{11} + T^n_{22}}{2}\right), \quad Z^n_{\text{eff}} = \sqrt{\frac{T^n_{12}}{T^n_{21}}}. \tag{6}$$

2.2 Visco-thermal losses model

The visco-thermal losses in the system are considered both in the Helmholtz resonators and in the slits by using its effective complex and frequency dependent parameters. Considering only plane waves propagate inside the metamaterial, the effective parameters of the ducts that conform 2D resonators and the slits of width $2r$ are given by [7]:

$$\rho_{\text{eff}} = \rho_0\left[1 - \frac{\tanh\left(rG_\rho\right)}{rG_\rho}\right]^{-1}, \quad \kappa_{\text{eff}} = \kappa_0\left[1 + (\gamma - 1)\frac{\tanh\left(rG_\kappa\right)}{rG_\kappa}\right]^{-1}, \tag{7}$$

with $G_\rho = \sqrt{i\omega\rho_0/\eta}$ and $G_\kappa = \sqrt{i\omega\text{Pr}\rho_0/\eta}$, and where γ is the specific heat ratio of air, P_0 is the atmospheric pressure, Pr is the Prandtl number, η the dynamic viscosity, ρ_0 the air density and $\kappa_0 = \gamma P_0$ the air bulk modulus. The effective parameters of the n-th main slit, $\rho^n_{\mathbf{s}}$ and $\kappa^n_{\mathbf{s}}$, are obtained by setting $r = h^n/2$ in Eqs. (7-7). The visco-thermal losses inside the 2-dimensional resonator's neck and cavity are modelled in the same way by these effective parameters, $\rho^{n,m}_{\mathbf{n}}$, $\kappa^{n,m}_{\mathbf{n}}$ and $\rho^{n,m}_{\mathbf{c}}$, $\kappa^{n,m}_{\mathbf{c}}$ respectively, by setting $r = w^{n,m}_{\mathbf{n}}/2$ and $r = w^{n,m}_{\mathbf{c}}/2$ for the m-th resonator located at the n-th slit.

2.3 Resonator impedance and end corrections

Using the effective parameters for the neck and cavity elements given by Eqs. (7-7), the impedance of a Helmholtz resonator, including a length correction due to the radiation can be written as [8]:

$$Z^{n,m}_{\text{HR}} = -i\frac{\cos(k_{\mathbf{n}}l_{\mathbf{n}})\cos(k_{\mathbf{c}}l_{\mathbf{c}}) - Z_{\mathbf{n}}k_{\mathbf{n}}\Delta l\cos(k_{\mathbf{n}}l_{\mathbf{n}})\sin(k_{\mathbf{c}}l_{\mathbf{c}})/Z_{\mathbf{c}} - Z_{\mathbf{n}}\sin(k_{\mathbf{n}}l_{\mathbf{n}})\sin(k_{\mathbf{c}}l_{\mathbf{c}})/Z_{\mathbf{c}}}{\sin(k_{\mathbf{n}}l_{\mathbf{n}})\cos(k_{\mathbf{c}}l_{\mathbf{c}})/Z_{\mathbf{n}} - k_{\mathbf{n}}\Delta l\sin(k_{\mathbf{n}}l_{\mathbf{n}})\sin(k_{\mathbf{c}}l_{\mathbf{c}})/Z_{\mathbf{c}} + \cos(k_{\mathbf{n}}l_{\mathbf{n}})\sin(k_{\mathbf{c}}l_{\mathbf{c}})/Z_{\mathbf{c}}}, \tag{8}$$

where (note superscripts were omitted for the sake of simplicity) $l^{n,m}_{\mathbf{n}}$ and $l^{n,m}_{\mathbf{c}}$ are the neck and cavity lengths, $k^{n,m}_{\mathbf{n}}$ and $k^{n,m}_{\mathbf{c}}$, are the effective wavenumbers and and $Z^{n,m}_{\mathbf{n}}$ and $Z^{n,m}_{\mathbf{c}}$ effective characteristic impedance in the neck and cavities respectively, and $\Delta l^{n,m}$ the correction length for the Helmholtz resonators. These correction lengths are deduced from the addition of two correction lengths $\Delta l^{n,m} = \Delta l^{n,m}_1 + \Delta l^{n,m}_2$ as

$$\Delta l^{n,m}_1 = 0.41\left[1 - 1.35\frac{w^{n,m}_{\mathbf{n}}}{w^{n,m}_{\mathbf{c}}} + 0.31\left(\frac{w^{n,m}_{\mathbf{n}}}{w^{n,m}_{\mathbf{c}}}\right)^3\right]w^{n,m}_{\mathbf{n}}, \tag{9}$$

$$\Delta l^{n,m}_2 = 0.41\left[1 - 0.235\frac{w^{n,m}_{\mathbf{n}}}{w^n_{\mathbf{s}}} - 1.32\left(\frac{w^{n,m}_{\mathbf{n}}}{w^n_{\mathbf{s}}}\right)^2 + 1.54\left(\frac{w^{n,m}_{\mathbf{n}}}{w^n_{\mathbf{s}}}\right)^3 - 0.86\left(\frac{w^{n,m}_{\mathbf{n}}}{w^n_{\mathbf{s}}}\right)^4\right]w^{n,m}_{\mathbf{n}}. \tag{10}$$

The first length correction, $\Delta l^{n,m}_1$, is due to pressure radiation at the discontinuity from the neck duct to the cavity of the Helmholtz resonator [9], while the second $\Delta l^{n,m}_2$ comes from the radiation at the discontinuity

from the neck to the principal waveguide [10]. This correction only depends on the radius of the waveguides, so it becomes important when the duct length is comparable to the radius, i.e., for small neck lengths and for frequencies where $k_{\mathbf{n}}^{n,m} w_{\mathbf{n}}^{n,m} \ll 1$.

Another important end correction comes from the radiation from the slits to the free air. The radiation correction for a periodic distribution of slits can be expressed as [11]:

$$\Delta l_{\text{slit}}^{n} = h^n \sigma^n \sum_{n=1}^{\infty} \frac{\sin^2(n\pi\sigma^n)}{(n\pi\sigma^n)^3}. \tag{11}$$

with $\sigma^n = h^n/d$. Note for $0.1 \leq \sigma^n \leq 0.7$ this expression reduces to $\Delta l_{\text{slit}}^{n} \approx -\sqrt{2}\ln\left[\sin\left(\pi\sigma^n/2\right)\right]/\pi$.

2.4 Diffusion coefficient

The diffusion coefficient, d_ϕ, is estimated from a polar response as [12]

$$\delta_\phi = \frac{\left(\int_{-\pi}^{\pi} I_s(\theta) d\theta\right)^2 - \int_{-\pi}^{\pi} I_s(\theta)^2 d\theta}{\int_{-\pi}^{\pi} I_s(\theta)^2 d\theta}, \tag{12}$$

where $I_s(\theta)$ is the polar scattering intensity for a wave with incident angle ϕ. This coefficient is normalized to that of a plane reflector, δ_{flat}, to eliminate the effect of the finite size of the structure as $\delta_n = (\delta_\phi - \delta_{\text{flat}})/(1 - \delta_{\text{flat}})$.

3 REDUCING THE THICKNESS OF A DIFFUSER USING METAMATERIALS

Figure 2 (a) shows the dispersion relations inside two different slits, $n = 1$ and $n = 2$, obtained by using $M = 2$ HR with the geometrical parameters listed in Table 1 of Ref. [13]. First, above the resonance frequency of the HRs, f_n, a band gap is generated. Below the resonance frequency of the HRs a dispersive band is observed and the wavenumber is increased with respect to the wavenumber in air. In this regime, slow sound conditions are produced, as shown in Fig. 2 (b), i.e., the phase speed inside the slits is strongly reduced. The phase of the reflection coefficient produced by each slit is shown in Fig. 2 (c). We can see that for some frequencies the phase of the reflection coefficient of both slits (blue and red lines) is strongly modified when compared to the reflection phase of a slit without HRs (dashed line). At 2 kHz, the 1st slit (red curve) reacts inverting the phase of the incoming wave, while for the 2nd slit (blue curve) this occurs at 3.2 kHz. In this way, by tuning the geometry a specific phase profile can be tailored, while the total thickness of the panel can be greatly reduced when compared with a quarter wavelength resonator of length L. By using these features, we show in this

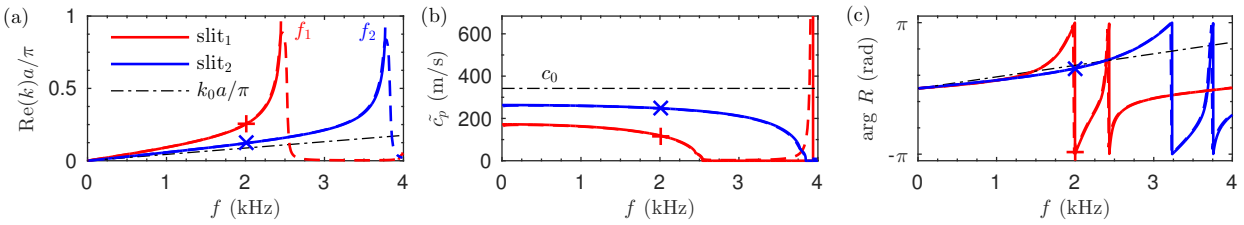


Figure 2. (a) Dispersion relation inside the (blue) first and (red) second slits of a metadiffuser for the lossless case (continuous lines) and accounting for the thermo-viscous losses (dashed lines), and wavenumber in air (dashed-dotted). The resonance frequencies of the HR are shown as f_1 and f_2. (b) Corresponding phase speed. (c) Phase of the reflection coefficient for each individual slit.

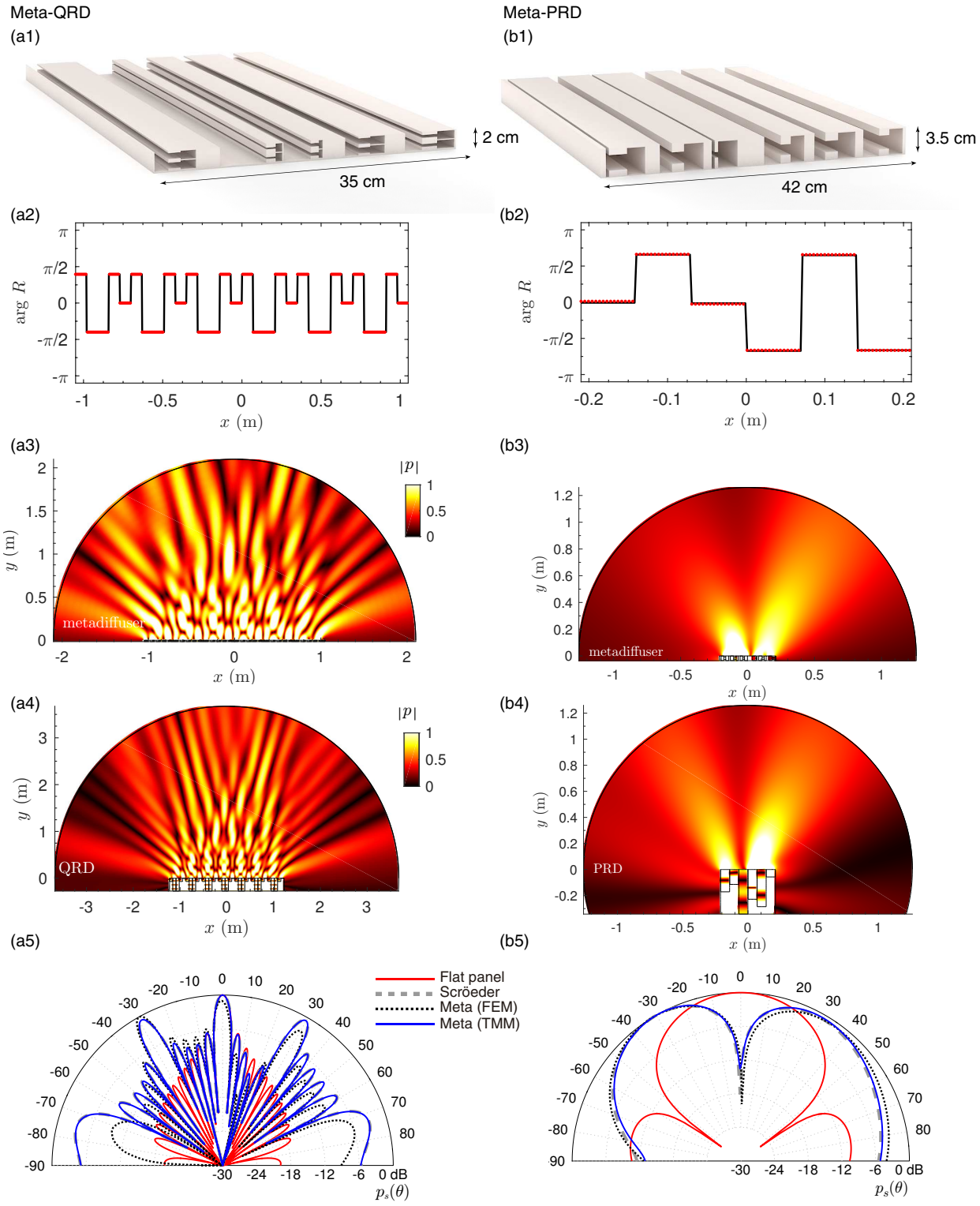


Figure 3. (a) Phase and (b) magnitude of the spatially-dependent reflection coefficient of a QRD (black line) and the QR-metadiffuser (red doted). (c) Scaled scheme of the QR-metadiffuser with $N = 5$ and $M = 2$. (d) Near field pressure distribution at 2 kHz of QR-metadiffuser with thickness $L = 2$ cm (e) phase grating QRD of thickness $L = 27.4$ cm and (f) flat plane reflector. (g) Far-field polar distribution of the QR-metadiffuser obtained by TMM (continuous blue) and FEM (dotted black), the reference QRD (dashed-grey), and a plane reflector with same width of the diffusers (continuous red).

article that the phase profile of Schroeder and ternary sequence diffusers can be mimicked by a sub-wavelength metadiffuser in a given frequency band. Therefore by tuning the geometry of a metadiffuser we can maximize sound diffusion in a broad frequency band for room acoustics applications using a deep sub-wavelength panel.

4 QUADRATIC RESIDUE METADIFFUSERS

The quadratic residue sequence is given by $s_n = n^2 \mathrm{mod} N$, where mod is the least non-negative remainder of the prime number N. If the phase grating diffuser is based on quarter wavelength resonators, the depth of the slits is given by $L_n = s_n \lambda_0 / 2N$, where λ_0 is the design wavelength. Here, we use optimization methods to tune the geometry of the metamaterial for its spatially-dependent reflection coefficient to match the one of regular QRD at single frequency. The resulting geometry is shown in Fig. 3 (a1). Figure 3 (a2) shows the phase of the reflection coefficient along the surface for a $N = 5$ QRD with a design frequency of 500 Hz and a total thickness of $L = 27.4$ cm, and a QR-metadiffuser of $L = 2$ cm thickness and $M = 2$ Helmholtz resonators of same dimensions, calculated using the transfer matrix method (TMM). Perfect agreement is found between the reflection coefficients of the QR-metadiffuser and the targeted phase grating QRD. The near field pressure distributions are shown in Figs. 3 (a3-a4) for the QR-metadiffuser and a QRD. Excellent agreement is observed between both diffusers, where it is clear how the field is scattered in other directions rather than specular one. Figure 3 (a5) shows the far-field calculation for both structures considering 6 repetitions of the unit cell in order to clearly generate the characteristic set of diffraction grating lobes of the QRD in the far-field. Excellent agreement is obtained with the polar response using the TMM and a full-wave numerical solution using the finite element method (FEM) accounting for the thermo-viscous losses. Notice that the presented QR-metadiffuser is 17.1 times thinner than the usual QRD (34 times smaller than the QRD design wavelength).

5 PRIMITIVE ROOT METADIFFUSERS

The second numerical sequence presented here is the primitive root sequence, given by $s_n = r^n \mathrm{mod} P$, where P is a prime number and r is the primitive root of P. The primitive root sequence have $N = P - 1$ different values. A primitive root diffuser (PRD) is constructed using a set of N wells with depths $L_n = s_n \lambda_0 / 2N$. The scattered field by these diffusers presents a notch at specular directions at multiples of the design frequency [14]. The obtained PR-metadiffuser design is shown in Figure 3 (b1) and the corresponding geometrical parameters of the PR-metadiffuser are listed in Table 2 of Ref.[13]. Figure 3 (b2) show both the phase of the spatially-dependent reflection coefficient of a $P = 7$ phase grating PRD of thickness $L = 17.1$ cm with $d = 7$ cm, and for a PR-metadiffuser of $L = 3.5$ cm and $M = 1$ HR with the same lateral dimensions. Excellent agreement is found between both responses. Figures 3 (b3-b4) show the near field corresponding to the PR-metadiffuser and a reference PRD. The characteristic notch is observed at normal reflection angle, i.e., $\theta = 0$. Note, because the structures are not symmetric, neither is the field. The far-field is presented in Fig. 3 (b5), where good agreement is found between the theory and the full-wave numerical solutions. Both panels produce the same scattering, but the thickness of the PR-metadiffuser is around 10 times thinner than the phase grating PRD (20 times smaller than the design wavelength).

6 BROADBAND OPTIMAL METADIFFUSERS

To obtain a metadiffuser useful for room acoustic applications, its diffusion must be broadened in frequency. Thus, we extend the bandwidth of the optimization procedure. In particular, we look for deep-subwavelength thickness metadiffusers presenting maximum normalized diffusion coefficient in the frequency range from 250 Hz to 2 kHz. A set of $N = 11$ slits separated by $d = 12$ cm was used, and the thickness of the panel was constrained to $L = 3$ cm. Figure 4 (a) shows the frequency dependent diffusion coefficient calculated according to ISO 17497-2:2012 normalized to a flat reflector of same dimensions for a thick QRD with a design frequency of 250 Hz ($L_{\mathrm{QRD}} = 56$ cm), a thin QRD with the same thickness of the metadiffuser $L_{\mathrm{QRD,thin}} = 3$ cm, and the

optimized metadiffuser. Over the optimized frequency range, the diffusion coefficient of the metadiffuser takes a mean value of $\delta_n \approx 0.65$, with peaks of $\delta_n = 0.91$. When compared to the thick QRD, its frequency band is extended to one octave below while the metadiffuser thickness is 46 times smaller than the wavelength.

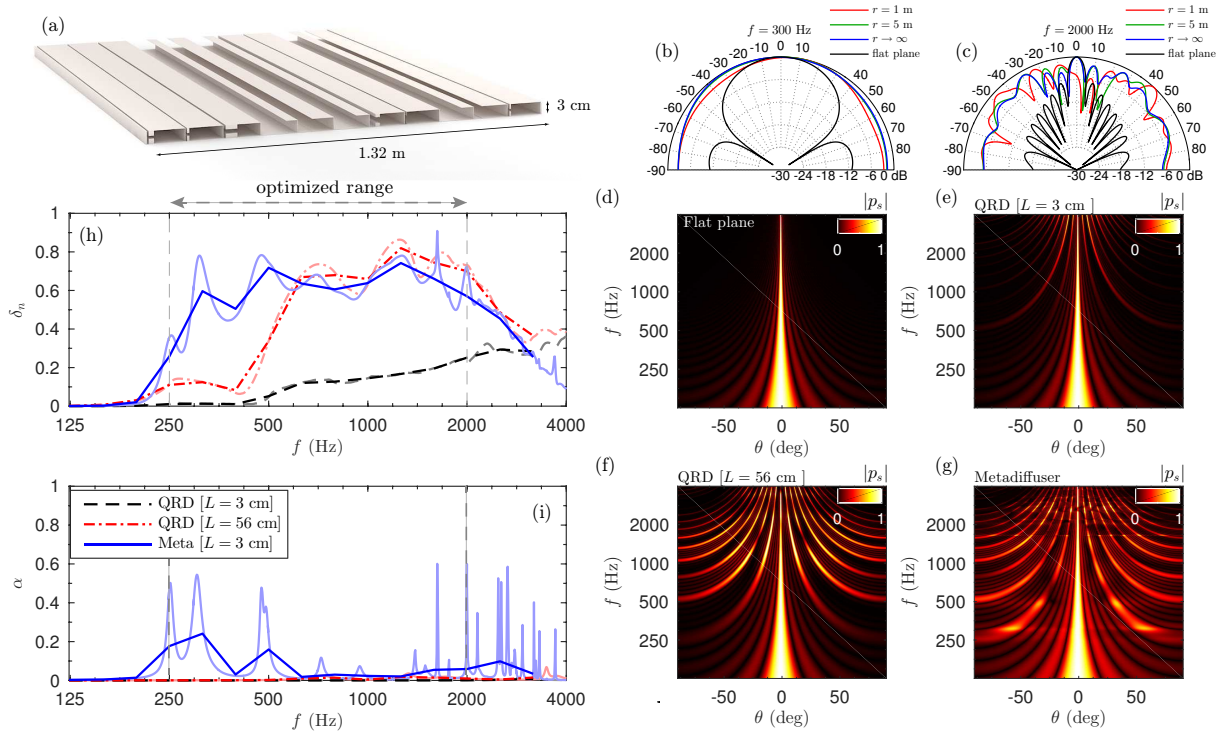


Figure 4. (a) Normalized diffusion coefficient of a 3 cm QRD (dashed black), 56 cm QRD (dashed-dotted red) and optimized metadiffuser using TMM (blue) integrated in third of octaves. The third octave integration is shown in thick lines according to ISO 17497-2:2012.

7 CONCLUSIONS

We have presented a novel concept of sound diffuser called *metadiffusers*. These new structures are based on metamaterials comprising slotted panel, with slits loaded by a set of Helmholtz resonators. The propagation inside each slit presents strong dispersion and the sound speed can be significantly reduced so that each slit effectively behaves as a deep-subwavelength resonator. Different designs were presented based on number-theoretical sequences as quadratic residue and primary root sequences. It was shown that the structures can be optimized to work in a broadband frequency range covering 3 octaves. In particular, we presented a 3 cm thick diffuser efficient from 250 to 2000 Hz, demonstrating the potential of the metadiffusers to be used in critical listening environments due to their deep-subwavelength nature: the thickness of the panel was 1/46 times the wavelength corresponding to the lowest working frequency, i.e., about a twenty times thinner than the traditional designs.

Finally, it should be remarked that the performance of the panel drops off at high frequency, which is not desirable for an acoustic diffuser high frequency diffusion prevents perceptual aberrations. This will be achieved in future studies by modifying the metamaterial structure.

ACKNOWLEDGEMENTS

This work was supported by Generalitat Valenciana through grant APOSTD/2017/042. The authors acknowledge financial support from COST Action DENORMS - CA15125, supported by COST (European Cooperation in Science and Technology).

REFERENCES

[1] Trevor J Cox and Peter D'Antonio. *Acoustic absorbers and diffusers: theory, design and application*. CRC Press, 3rd edition, 2016.

[2] Manfred R Schröder. Diffuse sound reflection by maximum- length sequences. *The Journal of the Acoustical Society of America*, 57(1):149–150, 1975.

[3] Noé Jiménez, Vicent Romero-García, Vincent Pagneux, and Jean-Philippe Groby. Quasiperfect absorption by subwavelength acoustic panels in transmission using accumulation of resonances due to slow sound. *Phys. Rev. B*, 95:014205, 2017.

[4] J-P Groby, R Pommier, and Y Aurégan. Use of slow sound to design perfect and broadband passive sound absorbing materials. *J. Acoust. Soc. Am.*, 139(4):1660–1671, 2016.

[5] N Jiménez, W Huang, V Romero-García, V Pagneux, and J-P Groby. Ultra-thin metamaterial for perfect and quasi-omnidirectional sound absorption. *Applied Physics Letters*, 109(12):121902, 2016.

[6] Noé Jiménez, Vicent Romero-García, Vincent Pagneux, and Jean-Philippe Groby. Rainbow-trapping absorbers: Broadband, perfect and asymmetric sound absorption by subwavelength panels for transmission problems. *Scientific reports*, 7(1):13595, 2017.

[7] Michael R Stinson. The propagation of plane sound waves in narrow and wide circular tubes, and generalization to uniform tubes of arbitrary cross-sectional shape. *J. Acoust. Soc. Am.*, 89(2):550–558, 1991.

[8] G Theocharis, O Richoux, V Romero García, A Merkel, and V Tournat. Limits of slow sound propagation and transparency in lossy, locally resonant periodic structures. *New J. Phys.*, 16(9):093017, 2014.

[9] J Kergomard and A Garcia. Simple discontinuities in acoustic waveguides at low frequencies: critical analysis and formulae. *J. Sound Vib.*, 114(3):465–479, 1987.

[10] Vincent Dubos, J Kergomard, A Khettabi, J-P Dalmont, DH Keefe, and CJ Nederveen. Theory of sound propagation in a duct with a branched tube using modal decomposition. *Acta Acustica united with Acustica*, 85(2):153–169, 1999.

[11] Fridolin P Mechel. *Formulas of acoustics, 2nd ed.* Springer Science & Business Media, 2008.

[12] ISO 17497–2:2012. Acoustics – Sound-scattering properties of surfaces – Part 2: Measurement of the directional diffusion coefficient in a free field. Iso standard, International Organization for Standardization, Geneva, Switzerland, 2012.

[13] Noé Jiménez, Trevor J Cox, Vicent Romero-García, and Jean-Philippe Groby. Metadiffusers: Deep-subwavelength sound diffusers. *Scientific reports*, 7(1):5389, 2017.

[14] Trevor J Cox and Peter D'Antonio. Acoustic phase gratings for reduced specular reflection. *Applied Acoustics*, 60(2):167–186, 2000.